Ultrasensitive detection of Ebola virus oligonucleotide based on upconversion nanoprobes/nanoporous membrane system

Ming-Kiu Tsang[1,$], WeiWei Ye[2,3,$], Guojing Wang[4], Jingming Li[4], Mo Yang[3], Jianhua Hao[1*]*

[1]M.-K. Tsang[$] and Prof. J. H. Hao*, Department of Applied Physics, The Hong Kong Polytechnic University, Hung Hom, Kowloon, Hong Kong (China)

[2]W. W. Ye[$], Institute of Ocean Research, Zhejiang University of Technology, Hangzhou, Zhejiang 310014, People's Republic of China

[3]W. W. Ye[$] and Prof. M. Yang*, Interdisciplinary Division of Biomedical Engineering , The Hong Kong Polytechnic University, Hung Hom, Kowloon, Hong Kong (China)

[4]G.Wang and J. Li, National Center for Clinical Laboratory, Beijing Hospital of the Ministry of Health, No. 1 Dahua Road, Dongdan, Beijing 100730, People's Republic of China

[$]Author Contributions: Ming-Kiu Tsang and WeiWei Ye contributed equally to this work

*E-mail: jh.hao@polyu.edu.hk and mo.yang@polyu.edu.hk

ABSTRACT: Ebola outbreaks are currently of great concern and therefore it is urgently needed to develop effective diagnosis methods. The key for lethal virus detection is high sensitivity, considering the early stage detection of virus may increase the probability of survival. Here we propose a novel luminescence scheme of assay consisted of $BaGdF_5$:Yb/Er upconversion nanoparticles (UCNPs) conjugated with oligonucleotide probe and gold nanoparticles (AuNPs) linked with target Ebola virus oligonucleotide. As a proof of concept, a homogeneous assay was fabricated and tested, yielding a detection limit at pM level. The luminescence resonance energy transfer is ascribed to the spectral overlapping of upconversion luminescence (UCL) and the absorption characteristics of AuNPs. Moreover, we anchored the UCNPs and AuNPs on a nanoporous alumina (NAAO) membrane to form a heterogeneous assay. Importantly, the detection limit was greatly improved, exhibiting a remarkable value at fM level. The enhancement is attributed to the increased light-matter interaction throughout the nanopore walls of NAAO membrane. The specificity test suggested that the nanoprobes were specific to Ebola virus oligonucleotides. The strategy combining UCNPs, AuNPs and NAAO membrane provides a new insight to low-cost, rapid and ultrasensitive detection of different diseases. Furthermore, we explored the feasibility of clinical application by using inactivated Ebola virus samples. The

detection results showed great potential of our heterogeneous design for practical application.

KEYWORDS: Upconversion, nanoprobe, biosensor, Ebola virus DNA, LRET

Ebola virus is a lethal pathogen and the recent outbreak spreads quickly into several countries with high fatality rate.[1,2] Hence, there is an urgent need to develop rapid and ultrasensitive bioassays for Ebola virus detection. The introduction of reverse transcription-polymerase chain reaction (RT-PCR),[3] and enzyme-linked immunosorbent assay (ELISA)[4] allow assays to be carried out with relatively safety. Target amplification based RT-PCR method has been implemented for Ebola detection. However, it suffers from drawbacks of expensive equipment, labor-intensive procedures, being time-consuming and susceptible to contamination during amplification process.[5] ELISA is a rapid alternative for Ebola virus detection, but the relatively low sensitivity and the need for high-quality sample preparation limit its applications for on-site detection.[6] Therefore, biosensors with both high sensitivity and rapid response are greatly desired for enabling rapid and sensitive detection of Ebola virus gene in a cost-effective way. The recently developed bio-barcode assay approaches,[7] optofluidic biosensors based on plasmonic nanoholes,[8] and interferometric measurement techniques[9] have been explored for Ebola virus gene

detection based on either complementary oligonucleotide (oligo) hybridization or antigen-antibody interaction. However, the fabrication processes for these biosensors are usually complicated and the sample preparation time is quite long.

Förster resonance energy transfer (FRET) biosensor, which generally includes an acceptor and a donor fluorophore, has been used for biosensing, bioassay, bioimaging, and photodynamic therapy.[10–12] Among those fluorescence sensors, lanthanide-doped upconversion nanoparticles (UCNPs) have emerged as alternatives over conventional down-shifting probes (organic dyes, quantum dots, etc.), and benefited from their unique merits for biodetection, including minimal background fluorescence, low photodamage, high photostability, large anti-Stokes shifts, and low toxicity.[13–16] The availability of relatively cheap and compact near-infrared (NIR) diode lasers as trigger sources further increases the convenience for on-site test. Hence, the UCNPs based assays feature high sensitivity, facile read-out and rapid detection.[17] As a result, various types of analytes, such as oxygen, temperature, fingerprints, ions, viruses and proteins,[18–27] have been successfully detected by using UCNPs-based biodetection systems. For instance, Chen *et al.* reported a dissolution-enhanced luminescent bioassay for carcinoembryonic antigen in human serum.[28] We have also reported a homogeneous assay for H7 subtype virus oligo detection.[29] Unfortunately, there has been no attempt to investigate the application of UCNPs for Ebola virus oligo

detection so far. In this work, we propose a novel strategy for Ebola virus oligo detection based on the luminescence resonance energy transfer (LRET) between UCNPs and AuNPs. Particularly, it is known that the desire for low limit of detection (LOD) of virus oligo detection is a prime objective when considering that cures can be administered at earlier stages to increase the probability of survival. Therefore, we have further demonstrated a heterogeneous assay of UCNPs and AuNPs on nanoporous alumina (NAAO) solid phase platform, allowing various molecules to be adsorbed on the nanoporous walls by covalent bonding because of easy surface modifications and high surface to volume ratio. As far as we know, the architecture combining UCNPs and NAAO has not yet been exploited. More importantly, our developed method can yield ultra-low LOD in fM level specific to Ebola virus oligo. Importantly, we further step forward to explore the possibility of using the heteroegenous design for clinical detection by using inactivated Ebola virus samples.

RESULTS AND DISCUSSION

Ebola target oligo detection based on LRET biosensor. Figure 1 shows the scheme for Ebola oligo detection in this work. Amino modified complementary oligo probes are immobilized on UCNPs. Under 980 nm diode laser excitation, the upconversion emissions of UCNPs are absorbed by AuNPs, leading to LRET process between

UCNPs and AuNPs conjugated with target Ebola virus oligo. Noted that the NIR-triggered nature of UCNPs possess low photodamage to the Ebola virus oligonucleotide hybridization with probe oligonucleotide. For a heterogeneous assay, APTES (3-Aminopropyltriethoxysilane) modified NAAO membranes are used for UCNPs conjugation with glutaraldehyde as the linkage molecule. High surface area to volume ratio of NAAO allows large amount of UCNPs to conjugate on the membrane surface. Oligo hybridization between complementary pairs can bring AuNPs to the proximity of UCNPs on NAAO membrane.

Characterizations of the UCNPs and the biodetection system. As a proof of concept, the PEI-modified $BaGdF_5$:Yb/Er UCNPs were synthesized by a one-pot hydrothermal method. Branched PEI molecules were used as capping agent to control the growth and enhance the water dispersity of the UCNPs. The selected area electron diffraction (SAED) pattern confirms the simple cubic structure of $BaGdF_5$:Yb/Er UCNPs (**Figure S1(a)**). The UCNPs present good water dispersity and the average size of the UCNPs was measured to be 14 nm (**Figure S1(b)**). The lattice spacing from high-resolution transmission electron microscopy (HRTEM) (**Figure S1(c)**) is estimated as 2.96 Å and it is consistent with the (200) of simple cubic structure of $BaGdF_5$ host. Moreover, the energy-dispersive X-ray (EDX) spectrum and elemental mapping (**Figure S1(d) and S2**) confirm the constitutional elements in $BaGdF_5$:Yb/Er

UCNPs, respectively. After conjugating the complementary probe onto PEI-modified UCNPs surface, a thin and non-crystalline layer can be observed in the HRTEM image (**Figure 2a**). The hybridization of the probe and the target resulted in the proximity of UCNPs and AuNPs. **Figure 2b** shows that the UCNP is surrounded by some AuNPs to form a satellite structure, manifesting the spatial configuration for LRET. Then, the UCNPs were anchored throughout the walls of NAAO pillows via the scheme as shown in **Figure 1** to form a heterogeneous assay. The typical structure of NAAO is shown in **Figure S3a**, revealing the cross-section of the arrays. **Figure 2c** indicates the presence of some small spherical-shaped particles the NAAO arrays. Then, EDX area scan was performed to confirm anchoring of UCNPs on the wall of the NAAO array (**Figure S3(b)**). When the target was added to the substrate, multi-layers are observed in **Figure 2d** because of hybridization between the probe and Ebola virus oligo. As a result, the walls of the NAAO arrays are covered by UCNPs and AuNPs.

On the other hand, **Figure S4(a)** presents X-ray diffraction (XRD) pattern of the $BaGdF_5$:Yb/Er UCNPs, which is consistent with the standard $BaGdF_5$ database (JCPDS 24-0098). The small shift in diffraction angle is due to the doping of Gd, Yb and Er^{3+} ions. After the conjugation of the probe, no observable change was found in the XRD pattern (**Figure S4(b)**), which indicates that the conjugation has no

influence on the crystalline structure. **Figure S4(c)** shows the XRD pattern after the hybridization of probe modified UCNPs and target-modified AuNPs. The peak marked with asterisk corresponds to the (111) of Au while the peak around 43° overlaps with the (200) of $BaGdF_5$:Yb/Er UCNPs.[29] The capping of the PEI molecules on the $BaGdF_5$:Yb/Er UCNPs surface is evident by FTIR (**Figure S5(a)**). The FTIR spectrum suggests the successful capping of PEI on the UCNPs. Followed by the capping, it is essential to modify the surface of UCNPs with a complementary probe for hybridizing the Ebola virus oligo. **Figure S5(b)** shows the FTIR spectrum of the sample with the probe modification. After modifying the probe oligo on the surface of UCNPs, the new bands at 1053 and 1224 cm^{-1} are seen due to C-O ribose and phosphate, respectively. The appearance of peaks at 1425, 1572, and 1649 cm^{-1} are the characteristic vibration bands of guanine base, cytosine base, and adenine bases, respectively. Therefore, these new peaks support the modification of the complementary probe on the UCNPs. The surface density of oligo probe is quantified by using fluorescence intensity characterization (**Figure S5(c)**). The decrease in the fluorescence intensity after conjugating FAM-oligo to UCNPs is used to calculate the surface density of oligo probe, which is estimated to be 30 oligo molecules per UCNP. Moreover, the zeta potential (ξ) of the PEI-modified UCNPs was measured as +30.2 mV (**Figure S5(d)**). The positive value is ascribed to the presence of NH_2^+ groups in

the capped PEI molecules. Upon the conjugation of the probe on the surface of the PEI molecules, ξ of the UCNPs changes to -32.6 mV, attributed from the negative charges in the capped oligo. In addition to UCNPs, the as-synthesized AuNPs present a ξ of -49.5 mV (**Figure S5(e)**), owing to the capping of the citrate stabilizing agent. After the conjugation of the Ebola virus oligos on the AuNPs, ξ shifts slightly to -11.8 mV due to the conjugation of Ebola virus oligos onto AuNPs. We employed the UV-vis technique to monitor the absorbance at 260 nm. The normalized absorbance of double-stranded oligo (dS-oligo) and dS-oligo with gold nanoparticle (dS-oligo-AuNPs) against temperature is shown in **Figure 3**. The sampling of data point is increased when the temperature is close to the melting point because the absorbance changes abruptly. The melting point of each type of dS-oligo corresponds to the absorbance value at 0.5. From the graph, the red line corresponds to the normalized absorbance of dS-oligo at 260 nm. The estimated melting point is about 58 ^{o}C. This value agrees very well with the data given by Integrated DNA Technologies (IDT) Inc. (Coralville, IA). After the conjugation of dS-oligo to AuNPs, the melting point increases to about 62 ^{o}C. The slight increment is ascribed to the change in ionic strength of the solution.

The UCNPs emit intense upconversion emission upon 980 nm laser excitation and three main emission bands were recorded at 523, 546 and 654 nm (**Figure S6**).

Meanwhile, the citrate stabilized AuNPs exhibit strong localized surface plasmonic resonance (LSPR) band with a peak absorption at about 523 nm (**Figure S7**). Hence, the spectral overlapping results in efficient LRET for Ebola virus detection. Owing to the good matching in optical spectra of UCNPs and AuNPs, the two kinds of nanoparticles were immobilized on the NAAO substrate in order to demonstrate the ultrasensitive detection capacity of the system. Noted that EDX is not applicable to precisely detect light elements (N, O, P, S, etc.), while X-ray photoelectron spectroscopy (XPS) can provide the information of light elements down to lithium instead. **Figure S8(a)** shows the XPS scan of the UCNPs-probe-Ebola oligo-AuNPs hybridized NAAO substrate. Most of the essential elements, such as Ba, Yb, Al and N, are present in the scan. Moreover, the high-resolution XPS (HR-XPS) scans as shown in **Figure S8(b)-(j)** reveal all the essential elements in the NAAO membrane based heterogeneous assay, such as P and S. Hence, this supported the hybrid combination of probe oligo conjugated with UCNPs and Ebola virus oligo conjugated with AuNPs on NAAO substrate.

LRET-based homogeneous and heterogeneous biodetection of Ebola oligo. The concentration of Ebola virus oligo on AuNPs was confirmed by using UV-vis spectroscopy. The optical density of Ebola virus oligo was taken at the wavelengths of 260 nm and the oligo concentration in the solution was calculated according to the

specification from IDT. It is estimated that there are 10 Ebola virus oligonucleotides per AuNP. Therefore, the concentration of Ebola virus oligo was quantified based on this number. **Figure 4a** presents a schematic comparison of the homogeneous and heterogeneous assay for Ebola virus oligo detection. On the left panel, the pink colloidal solution consists of the hybridized probes and targets. Subsequently, green upconversion luminescence (UCL) emission was observed by naked eyes as a result of 980 nm laser excitation. Meanwhile, the middle upper and lower panels show the probe-modified UCNPs (pale white) and as-hybridized heterogeneous system (pink) on NAAO membrane, respectively. The corresponding confocal microscopy images show the comparison of the two UCL emissions of before (right upper image) and after (right lower image) hybridized systems under 980 nm laser excitation. It is apparent that the hybridization of AuNP-Ebola virus oligo results in much weaker UCL emission. For the quantitative studies, first we measured the UCL spectra of $BaGdF_5$:Yb/Er UCNPs in the homogeneous assay at different concentrations of Ebola virus oligos (**Figure 4b**). The control (Ctrl) spectrum was recorded by using 200 μg ml^{-1} UCNPs. The UCL intensities decrease with increasing oligo concentrations, attributed to the complete hybridization of the complementary probe and Ebola virus oligo. As shown in **Figure 4c**, the quenching efficiency monitored at 546 nm increases sharply from 3 pM and the curve saturates until 5 nM. The maximum

quenching efficiency is about 0.8. To prove the improved LOD of nanoprobes using NAAO, the above system was transferred to the NAAO membrane to form a heterogeneous assay. NAAO has previously been used for biosensors to detect bovine serum albumin, virus and DNA[30–32] with the advantages of simple fabrication process and low cost. In principle, this type of assay has the potential of enhancing the detection sensitivity due to the strong binding of the target and capturing molecules on the solid substrate.[17] Moreover, the three-dimensional (3D) array structures in NAAO can also enhance the sensitivity of biosensors because the target and capturing molecule are anchored throughout the wall of the pillows.[33] For comparison, the same anchoring procedures were carried out on a piece of ordinary aluminum oxide (ALO) foil. The UCL on the NAAO substrate recorded a 6-fold enhancement compared to that on ALO foil (**Figure S9**). Therefore, we attribute this phenomenon to the increased capturing of UCNPs over the thickness of the 3D NAAO arrays, and consequently more UCNPs can be excited to emit more intense UCL emission. In the heterogeneous assay based on NAAO, the same concentration of UCNPs was used for fair comparison. As anticipated, the UC emission decreases with increasing concentrations of Ebola virus oligos (**Figure 4d**) and the quenching efficiency is around 0.88 (**Figure 4e**). Therefore, the NAAO membrane based LRET biosensor with UCNPs and AuNPs as donors and acceptors provides a simple and rapid

platform for Ebola virus oligo detection. After hybridization, the UCNPs and AuNPs were situated in close proximity; hence the UCL emission was efficiently quenched by AuNPs. It should be mentioned that the short reaction time and easy operation of the nanoprobe are advantageous to the detection compared to the existing detection methods, such as RT-PCR and ELISA.

Figure of merit of the biosensor system. The qualities of biosensors are usually characterized by the linear response, LOD and specificity. **Figure S10(a)** shows UCL quenching against the concentrations of Ebola virus oligo in the homogeneous assay. The quenching efficiency increases with increasing target Ebola virus oligo concentrations. Accordingly, a linear response is found from 3 pM to 50 pM, which is suitable to serve as a biosensor for detecting Ebola virus oligo. The linear relationship between the quenching efficiency and concentration was plotted in **Figure S10(b)**, fitted as $y = 0.075 \ln(x) + 0.449$ and the LOD is estimated at about 7 pM. **Figure 5a** shows similar quenching effect as observed in the heterogeneous assay using NAAO substrate. Importantly, the linear response can be improved from pM to fM level ranging from 50 fM to 700 fM. The linear relationship is fitted as $y = 0.0003 x + 0.0163$ (**Figure 5b**). The LOD can be calculated to be about 300 fM, implying a significant improvement of about 30-fold compared to the homogeneous assay. Such a comparative study indicates that the scheme of heterogeneous assay using NAAO

membrane can largely enhance the sensitivity of Ebola virus gene detection. The enhancement is mainly due to the high cross-sectional area of the 3D NAAO pillows in the nanoporous membrane. These pillows increased the capturing of UCNPs and targets throughout the wall, hence the increment in light-matter interaction accounts for the improvement in LOD. Furthermore, the specificity which reflects the capability of the system to recognize a specific target molecule is of paramount importance in biosensing technology. To investigate the specificity of the two types of biosensor, 3 nM of target Ebola virus oligo, 3-base mismatch oligo and non-complementary oligo were tested for homogeneous assay, while the concentration for heterogeneous assay is 500 fM because this concentration is in the linear detection range of this LRET biosensor. **Figure S10(c)** and **5c** correspond to the results of specificity test for homogeneous and heterogeneous assay, respectively. Both results suggest that the 3-base mismatch target and non-complementary target present lower quenching efficiency compared to the Ebola virus oligo targets. Therefore, the proposed assay in this work is an ultrasensitive and specific biosensor for the detection of Ebola virus oligo.

Despite the rapid development of upconversion based biosensors, there is limited report on demonstrating clinical applications. Here we further explored the possibility of using the novel heterogeneous assay for clinical sample detection. Here, inactivated

Ebola virus samples obtained from Beijing hospital were used for clinical detection. Prior to extraction of target Ebola viral RNA, human serum was added to the inactivated Ebola virus samples to simulate the infected samples from the patients. Then, the RNA target was extracted by using PureLink Viral RNA kit (Life Technologies) according to the manufacturer's protocol. **Figure 6(a)** shows the UCL spectra of the heterogeneous LRET assays at various concentrations of the RNA target extracted from inactivated Ebola virus**. Figure 6(b)** presents the respective quenching efficiency against different extracted viral RNA concentrations. The results show that the heterogeneous system performs well for extracted viral RNA in the range of pM to fM level. Notably, the concentration of Ebola viral RNA extracted from can be detected as low as 500 fM, which is among the range of previously reported clinical detection using traditional methods.[34] Hence, these results indicate our heterogeneous design has the great potential for clinical detection of real samples in the future. The viral RNA extraction equipment should be kept clean during the extraction procedures to avoid potential RNase contamination, which may affect the conjugation of the target RNA with AuNPs and hence, decrease the sensitivity of the biosensor. In contrast to well-established technique, such as RT-PCR and ELISA, our method requires no thermal cycling and the preparation time is relatively short because of no requirement in amplification. In our experiment, oligonucleotides were extracted from

inactivated virus particle samples by PureLink Viral RNA kit and used for detection without amplification process. The detailed inactivated virus particle preparation and viral RNA extraction procedures are referred to supporting document. The preparation time mainly depends on oligonucleotide extraction procedure which can be quickly finished within 45 min by a commercialized kit. In addition, the readout of LRET luminescence signal is easy which makes our LRET assay suitable for on-site detection. Finally, LRET assays are well known for their high sensitivity to detect biological interaction at nanoscale, which brings high sensitivity to our LRET assay without amplification. In terms of LOD, the unit for RT-PCR is usually thousands of copies/mL[35,36] and it is possible to convert the copies/mL unit to molarity. After conversion, the LOD from RT-PCR is also at fM level. Hence, our heterogeneous assay has a comparable LOD with the RT-PCR technique. Moreover, compared to other reported biosensors, such as optofluidic biosensors based on plasmonic nanoholes[8], and interferometric measurement techniques,[9] our technique requires no complex fabrication technique but only slight chemical modifications for capturing the target. In addition to biosensor design, recent report shows that core-shell UCNPs structure can reduce unwanted cell-particle interaction in long term biological experiments,[37] which could be used for further enhancement in nanoprobe performance. Nevertheless, it is still important to develop more novel methods for

detecting Ebola virus oligo because multi-detection methods can avoid false-positive signal from a signal detection method.

CONCLUSIONS

In summary, we have firstly developed lanthanide-doped upconversion nanoprobes for ultrasensitive detection of Ebola virus oligonucleotide. Owing to the probe-target hybridization, the UCL emission is quenched by AuNPs with increasing target concentrations. A novel heterogeneous assay has been developed by immobilizing UCNPs and AuNPs on the NAAO membranes. Compared to the homogeneous assay, the LOD of the heterogeneous assay is significantly improved, which can reach down to fM level. We have also explored clinical detection using inactivated Ebola virus samples whose detection limit can also reach fM level. The results indicate our biosensor has the great potential for future clinical detection. Such a heterogeneous design may be generally expanded to various diseases detection based on luminescent nanoprobes. This work will open up the new possibilities for early stage detection of Ebola virus via upconversion luminescence routes.

Methods

One-pot hydrothermal synthesis of PEI-capped $BaGdF_5$:Yb/Er UCNPs. PEI-modified $BaGdF_5$:Yb/Er UCNPs with high monodispersity were synthesized according to previously reported hydrothermal synthesis.[29,38,39] Typically, 1.0 g of PEI was added to 20 ml of EG with 1 mmol of lanthanide dopants, 0.5 M $Gd(NO_3)_3$, $Yb(NO_3)_3$ and 0.1 M $Er(NO_3)_3$ with a molar ratio of 78:20:2 under vigorous mixing. 1 mmol of $BaCl_2$ was added to the above solution. The mixture was agitated for 30 min to form a transparent homogenous solution. Then, 5.5 mmol of NH_4F in 10 ml of EG was added to the above mixture. The mixture was agitated for 1 h and subsequently transferred to a 50 ml stainless steel Telfon-lined autoclave and hydrothermal at 190 ^oC for 24 h. After reaction, the as-synthesized UCNPs were separated from the reaction mixture by centrifugation, washed several times by ethanol and DI water. Finally, the UCNPs were dried in vacuum at 60 ^oC for 24 h.

Characterizations. Powder X-ray diffraction (XRD) patterns of the as-prepared UCNPs were recorded using a Rigaku smart lab 9 kW (Rigaku, Japan) with Cu K_α radiation (λ = 1.5406 Å). The shape, size and structure of the as-prepared PEI-$BaGdF_5$:Yb/Er UCNPs and AuNPs were characterized by using JEOL-2100F transmission electron microscopy (TEM) equipped with an Oxford Instrument energy-dispersive X-ray (EDX) spectrometry system, operating at 200 kV. The

crystal structure of the UCNPs was characterized by selected area electron diffraction (SAED). Samples for TEM were prepared on holey carbon coated 400 mesh copper grids. Fourier transform infrared spectrum (FTIR) was recorded by a PerkinElmer Spectrum 100 FT-IR spectrometer (PerkinElmer Inc., USA). Zeta potential measurements were performed on a Zetasizer Zeta Potential Analyzer (Malvern Instruments Ltd., England). Amino and fluorescein modified oligonucleotide probes with 25 bases were covalently conjugated to UCNPs and the fluorescence intensity was measured by a Microplate Reader (Infinite F200, Tecan, Switzerland). The scan was taken for three times and the zeta potential values were averaged. X-ray photoelectron spectroscopy (XPS) analysis was conducted on the system of Sengyang SKL-12 electron spectrometer equipped with a VG CLAM 4MCD electron energy analyzer. Al Kα source (1253.6 eV) operated with an accelerating voltage of 10 kV and emission current of 15 mA. Upconversion emission spectra were recorded using FLS920P Edinburgh Analytical Instrument apparatus equipped with an excitation source of CW 980 nm diode laser. Confocal optical micrographs of NAAO were obtained from a confocal laser scanning microscope, Leica TCS SP5, equipped with a Ti:Sapphire laser (Libra II, Coherent).

ACKNOWLEGMENTS

This work was supported by the Hong Kong PhD Fellowship Scheme Fund, National Natural Science Foundation of China (Project No: 81471747 and 11474241), PolyU grant (4-BCAG), CAS/SAFEA International Partnership Program for Creative Research Teams and Innovation and Technology Support Programme (Project No. ITS/057/15).

Supporting information.

This material is available free of charge via the Internet at http://pubs.acs.org.

REFERENCES

(1) Gire, S. K.; Goba, A.; Andersen, K. G.; Sealfon, R. S. G.; Park, D. J.; Kanneh, L.; Jalloh, S.; Momoh, M.; Fullah, M.; Dudas, G.; *et al.* Genomic Surveillance Elucidates Ebola Virus Origin and Transmission during the 2014 Outbreak. *Science.* **2014**, *345*, 1369–1372.

(2) World Health Organization. Ebola Situation Report. *Ebola response roadmap* **2015**, 1–13.

(3) Sanchez, A.; Ksiazek, T. G.; Rollin, P. E.; Miranda, M. E. G.; Trappier, S. G.; Khan, A. S.; Peters, C. J.; Nichol, S. T. Detection and Molecular Characterization of Ebola Viruses Causing Disease in Human and Nonhuman Primates. *J. Infect. Dis.* **1999**, *179*, S164–S169.

(4) Traf, U.; Sullivan, N. J.; Sanchez, A.; Rollin, P. E.; Yang, Z.; Nabel, G. J. Development of a Preventive Vaccine for Ebola Virus Infection in Primates. *Nature* **2000**, *408*, 605–609.

(5) Jones, S. M.; Feldmann, H.; Ströher, U.; Geisbert, J. B.; Fernando, L.; Grolla, A.; Klenk, H.-D.; Sullivan, N. J.; Volchkov, V. E.; Fritz, E. A.; *et al.* Live

Attenuated Recombinant Vaccine Protects Nonhuman Primates against Ebola and Marburg Viruses. *Nat. Med.* **2005**, *11*, 786–790.

(6) Sullivan, N. J.; Geisbert, T. W.; Geisbert, J. B.; Xu, L.; Yang, Z.; Roederer, M.; Koup, R. A.; Jahrling, P. B.; Nabel, G. J. Accelerated Vaccination for Ebola Virus Haemorrhagic Fever in Non-Human Primates. *Nature* **2003**, *424*, 681–684.

(7) Li, Y.; Cu, Y. T. H.; Luo, D. Multiplexed Detection of Pathogen DNA with DNA-Based Fluorescence Nanobarcodes. *Nat. Biotechnol.* **2005**, *23*, 885–889.

(8) Yanik, A. A.; Huang, M.; Kamohara, O.; Artar, A.; Geisbert, T. W.; Connor, J. H.; Altug, H. An Optofluidic Nanoplasmonic Biosensor for Direct Detection of Live Viruses from Biological Media. *Nano Lett.* **2010**, *10*, 4962–4969.

(9) Daaboul, G. G.; Lopez, C. A.; Chinnala, J.; Goldberg, B. B.; Connor, J. H.; Unlü, M. S. Digital Sensing and Sizing of Vesicular Stomatitis Virus Pseudotypes in Complex Media: A Model for Ebola and Marburg Detection. *ACS Nano* **2014**, *8*, 6047–6055.

(10) Jares-Erijman, E. A.; Jovin, T. M. FRET Imaging. *Nat. Biotechnol.* **2003**, *21*, 1387–1395.

(11) Samia, A. C. S.; Chen, X.; Burda, C. Semiconductor Quantum Dots for Photodynamic Therapy. *J. Am. Chem. Soc.* **2003**, *125*, 15736–15737.

(12) Klostermeier, D.; Sears, P.; Wong, C.-H.; Millar, D. P.; Williamson, J. R. A Three-Fluorophore FRET Assay for High-Throughput Screening of Small-Molecule Inhibitors of Ribosome Assembly. *Nucleic Acids Res.* **2004**, *32*, 2707–2715.

(13) Tsang, M.-K.; Bai, G.; Hao, J. Stimuli Responsive Upconversion Luminescence Nanomaterials and Films for Various Applications. *Chem. Soc. Rev.* **2015**, *44*, 1585–1607.

(14) Han, S.; Deng, R.; Xie, X.; Liu, X. Enhancing Luminescence in Lanthanide-Doped Upconversion Nanoparticles. *Angew. Chem. Int. Ed.* **2014**, *53*, 11702–11715.

(15) Gai, S.; Li, C.; Yang, P.; Lin, J. Recent Progress in Rare Earth Micro/nanocrystals: Soft Chemical Synthesis, Luminescent Properties, and Biomedical Applications. *Chem. Rev.* **2014**, *114*, 2343–2389.

(16) Haase, M.; Schäfer, H. Upconverting Nanoparticles. *Angew. Chem. Int. Ed.* **2011**, *50*, 5808–5829.

(17) Zheng, W.; Huang, P.; Tu, D.; Ma, E.; Zhu, H.; Chen, X. Lanthanide-Doped Upconversion Nano-Bioprobes: Electronic Structures, Optical Properties, and Biodetection. *Chem. Soc. Rev.* **2015**, *44*, 1379–1415.

(18) Wu, S.; Duan, N.; Ma, X.; Xia, Y.; Yu, Y.; Wang, Z.; Wang, H. Simultaneous Detection of Enterovirus 71 and Coxsackievirus A16 Using Dual-Colour Upconversion Luminescent Nanoparticles as Labels. *Chem. Commun.* **2012**, *48*, 4866–4868.

(19) Wu, S.; Duan, N.; Shi, Z.; Fang, C.; Wang, Z. Simultaneous Aptasensor for Multiplex Pathogenic Bacteria Detection Based on Multicolor Upconversion Nanoparticles Labels. *Anal. Chem.* **2014**, *86*, 3100–3107.

(20) Wu, L.; Wang, J.; Yin, M.; Ren, J.; Miyoshi, D.; Sugimoto, N.; Qu, X. Reduced Graphene Oxide Upconversion Nanoparticle Hybrid for Electrochemiluminescent Sensing of a Prognostic Indicator in Early-Stage Cancer. *Small* **2014**, *10*, 330–336.

(21) Ding, Y.; Zhu, H.; Zhang, X.; Zhu, J.-J.; Burda, C. Rhodamine B Derivative-Functionalized Upconversion Nanoparticles for FRET-Based Fe(3+)-Sensing. *Chem. Commun.* **2013**, *49*, 7797–7799.

(22) Liu, Y.; Chen, M.; Cao, T.; Sun, Y.; Li, C.; Liu, Q.; Yang, T.; Yao, L.; Feng, W.; Li, F. A Cyanine-Modified Nanosystem for in Vivo Upconversion Luminescence Bioimaging of Methylmercury. *J. Am. Chem. Soc.* **2013**, *135*, 9869–9876.

(23) Achatz, D. E.; Meier, R. J.; Fischer, L. H.; Wolfbeis, O. S. Luminescent Sensing of Oxygen Using a Quenchable Probe and Upconverting Nanoparticles. *Angew. Chem. Int. Ed.* **2011**, *50*, 260–263.

(24) Wang, J.; Wei, T.; Li, X.; Zhang, B.; Wang, J.; Huang, C.; Yuan, Q. Near-Infrared-Light-Mediated Imaging of Latent Fingerprints Based on Molecular Recognition. *Angew. Chem. Int. Ed.* **2014**, *53*, 1616–1620.

(25) Liu, J.; Liu, Y.; Bu, W.; Bu, J.; Sun, Y.; Du, J.; Shi, J. Ultrasensitive Nanosensors Based on Upconversion Nanoparticles for Selective Hypoxia Imaging in Vivo upon near-Infrared Excitation. *J. Am. Chem. Soc.* **2014**, *136*, 9701–9709.

(26) Vetrone, F.; Naccache, R.; Zamarrón, A.; Juarranz de la Fuente, A.; Sanz-Rodríguez, F.; Martinez Maestro, L.; Martín Rodriguez, E.; Jaque, D.; García Solé, J.; Capobianco, J. A. Temperature Sensing Using Fluorescent Nanothermometers. *ACS Nano* **2010**, *4*, 3254–3258.

(27) Huang, P.; Zheng, W.; Zhou, S.; Tu, D.; Chen, Z.; Zhu, H.; Li, R.; Ma, E.; Huang, M.; Chen, X. Lanthanide-Doped LiLuF4 Upconversion Nanoprobes for the Detection of Disease Biomarkers. *Angew. Chemie Int. Ed.* **2014**, *53*, 1252–1257.

(28) Zhou, S.; Zheng, W.; Chen, Z.; Tu, D.; Liu, Y.; Ma, E.; Li, R.; Zhu, H.; Huang, M.; Chen, X. Dissolution-Enhanced Luminescent Bioassay Based on Inorganic Lanthanide Nanoparticles. *Angew. Chem. Int. Ed.* **2014**, *53*, 12498–12502.

(29) Ye, W. W.; Tsang, M.-K.; Liu, X.; Yang, M.; Hao, J. Upconversion Luminescence Resonance Energy Transfer (LRET)-Based Biosensor for Rapid and Ultrasensitive Detection of Avian Influenza Virus H7 Subtype. *Small* **2014**, *10*, 2390–2397.

(30) Chan, K. Y.; Ye, W. W.; Zhang, Y.; Xiao, L. D.; Leung, P. H. M.; Li, Y.; Yang, M. Ultrasensitive Detection of E. Coli O157:H7 with Biofunctional Magnetic Bead Concentration via Nanoporous Membrane Based Electrochemical Immunosensor. *Biosens. Bioelectron.* **2013**, *41*, 532–537.

(31) Hotta, K.; Yamaguchi, A.; Teramae, N. Nanoporous Waveguide Sensor with Optimized Nanoarchitectures for. *ACS Nano* **2012**, 1541–1547.

(32) Feng, C.-L.; Zhong, X. H.; Steinhart, M.; Caminade, A. M.; Majoral, J.-P.; Knoll, W. Graded-Bandgap Quantum- Dot-Modified Nanotubes: A Sensitive Biosensor for Enhanced Detection of DNA Hybridization. *Adv. Mater.* **2007**, *19*, 1933–1936.

(33) Kang, M.; Trofin, L.; Mota, M. O.; Martin, C. R. Protein Capture in Silica Nanotube Membrane 3-D Microwell Arrays. *Anal. Chem.* **2005**, *77*, 6243–6249.

(34) WHO Ebola Response Team. Ebola Virus Disease in West Africa — The First 9 Months of the Epidemic and Forward Projections. *N. Engl. J. Med.* **2014**, *371*, 1481–1495.

(35) Drosten, C.; Drosten, C.; Schilling, S.; Schilling, S.; Asper, M.; Asper, M.; Panning, M.; Panning, M.; Schmitz, H.; Schmitz, H. Rapid Detection and Quantification of RNA of Ebola and Marburg Viruses, Lassa Virus, Crimean-Congo Hemorrhagic Fever Virus, Rift Valley Fever Virus, Dengue Virus, and Yellow Fever Virus by Real-Time Reverse Transcription-PCR. *J. Clin. Microbiol.* **2002**, *40*, 2323–2330.

(36) Towner, J. S.; Rollin, P. E.; Bausch, D. G.; Sanchez, A.; Crary, S. M.; Vincent, M.; Lee, F.; Spiropoulou, C. F.; Ksiazek, T. G.; Lukwiya, M.; *et al.* Rapid Diagnosis of Ebola Hemorrhagic Fever by Reverse Transcription-PCR in an Outbreak Setting and Assessment of Patient Viral Load as a Predictor of Outcome. *J. Virol.* **2004**, *78*, 4330–4341.

(37) Tian, J.; Zeng, X.; Xie, X.; Han, S.; Liew, O.; Chen, Y.; Wang, L.; Liu, X. Intracellular Adenosine Triphosphate Deprivation through Lanthanide-Doped Nanoparticles. *J. Am. Chem. Soc.* **2015**, *137*, 6550–6558.

(38) Zeng, S.; Tsang, M.-K.; Chan, C.-F.; Wong, K.-L.; Hao, J. PEG Modified $BaGdF_5$:Yb/Er Nanoprobes for Multi-Modal Upconversion Fluorescent, in Vivo X-Ray Computed Tomography and Biomagnetic Imaging. *Biomaterials* **2012**, *33*, 9232–9238.

(39) Zeng, S.; Tsang, M.-K.; Chan, C.-F.; Wong, K.-L.; Fei, B.; Hao, J. Dual-Modal Fluorescent/magnetic Bioprobes Based on Small Sized Upconversion Nanoparticles of Amine-Functionalized $BaGdF_5$:Yb/Er. *Nanoscale* **2012**, *4*, 5118–5124.

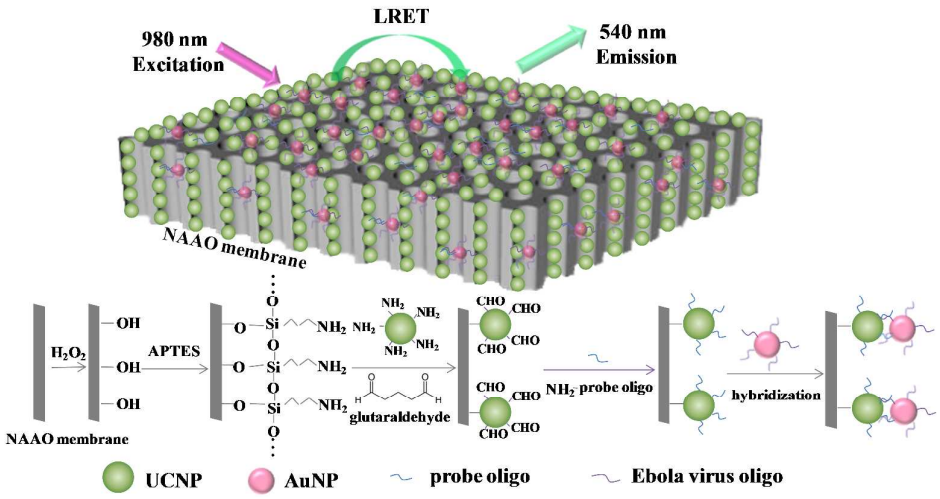

Figure 1. Schematic diagram of Ebola target oligo detection based on LRET biosensor with energy transfer from UCNPs to AuNPs on NAAO membrane.

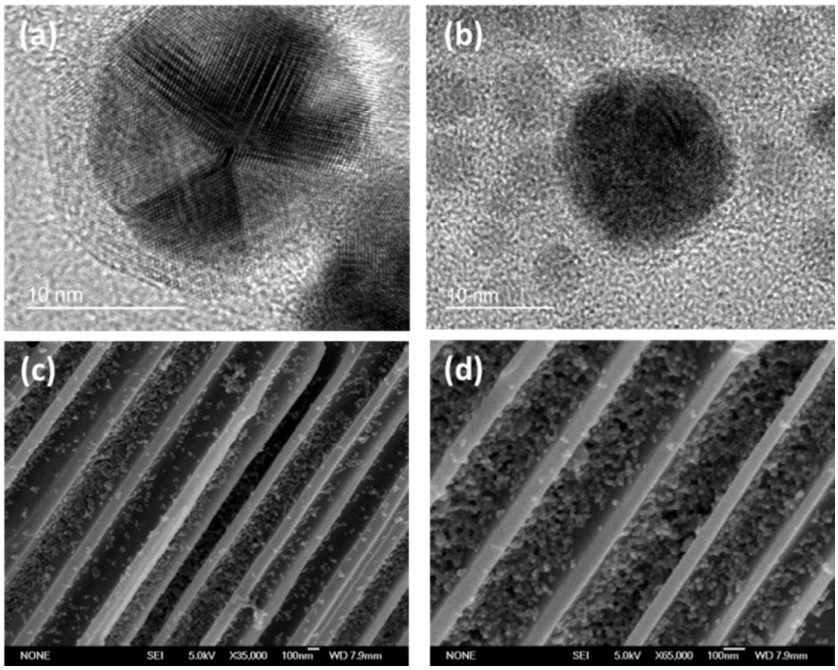

Figure 2. (a) HRTEM of a probe-modified $BaGdF_5$:Yb/Er UCNPs; (b) HRTEM of the satellite structure as a result of oligo hybridization of probe-modified UCNPs and AuNPs; FE-SEM of (c) The NAAO arrays with $BaGdF_5$:Yb/Er UCNPs anchored on the thickness of the arrays; (d) The NAAO arrays with UCNPs-probe-Ebola virus oligo-AuNPs covering most part of the arrays. The scale bars for TEM and SEM are 10 nm and 100 nm, respectively.

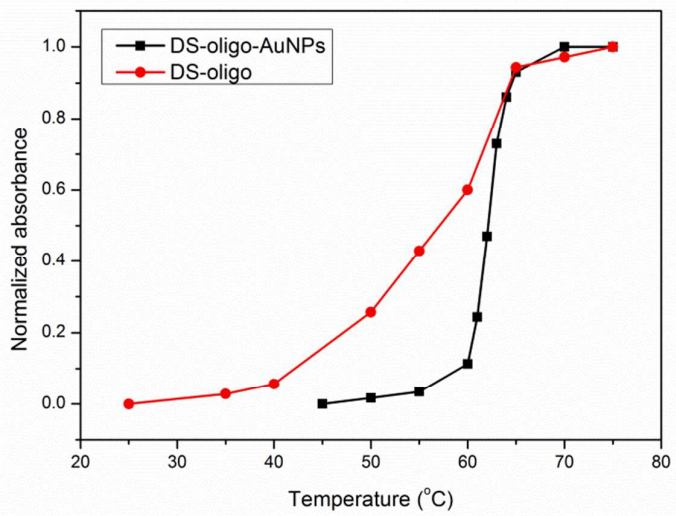

Figure 3. UV melting curves for DNA duplex (DS-oligo) and double-stranded DNA attached to gold nanoparticles (DS-oligo-AuNPs) at 260 nm.

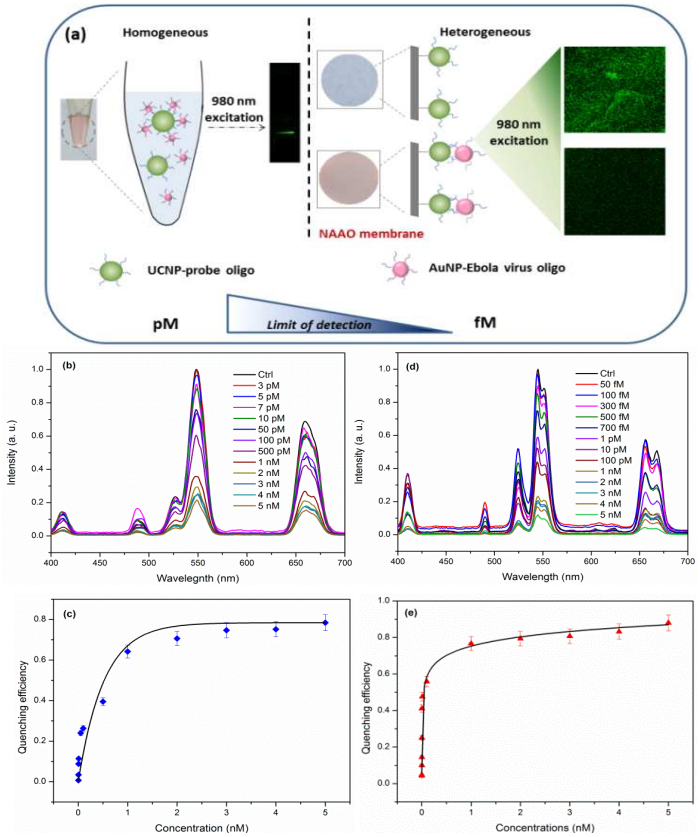

Figure 4. (a) Comparison of the homogeneous and heterogeneous assays for Ebola virus oligo detection; (b) UC emission spectra of $BaGdF_5$:Yb/Er-probe UCNPs with various concentration of Ebola virus oligo target in the homogeneous assay; (c) Quenching efficiency with different concentrations of Ebola virus oligo target in the homogeneous assay; (d) UC emission spectra of $BaGdF_5$:Yb/Er-probe UCNPs with various concentration of Ebola virus oligo target in the heterogeneous assay with NAAO membrane; (e) Quenching efficiency with virus oligo in the heterogeneous assay with NAAO membrane.

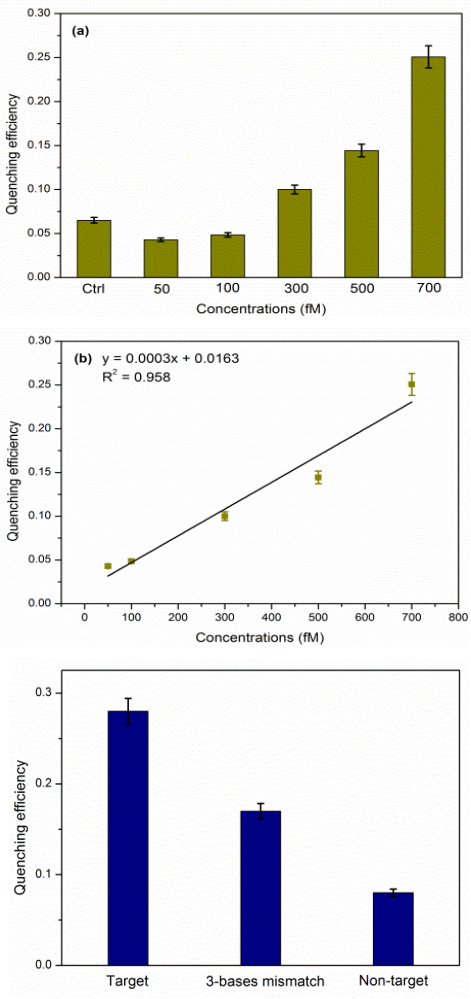

Figure 5. (a) UCL quenching efficiency against different concentration of Ebola virus oligo from 50 fM to 700 fM in the heterogeneous assay; (b) Linear relationship of the heterogeneous assay for Ebola virus oligo; (c) Specificity test of the heterogeneous assay for Ebola virus oligo detection based on a 3-bases mismatch gene and a non-complementary target at 500 fM target concentration. The LOD is estimated by including the control signal with three times of standard deviation.

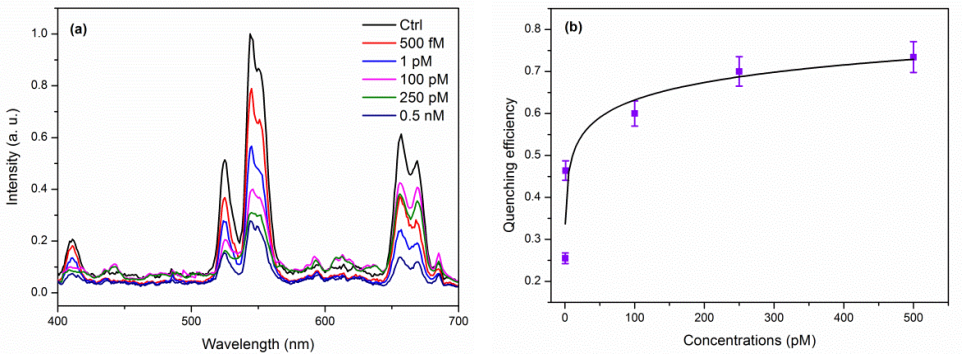

Figure 6. (a) Upconversion emission spectra and (b) Quenching efficiency of extracted RNA from inactivated Ebola virus like particles detection in the homogeneous assay system.

TOC

Ultrasensitive detection of Ebola virus oligonucleotide based on upconversion nanoprobes/nanoporous membrane system